Editors' Suggestion

Synthesis of osmium hydride under high hydrogen pressure

Mikhail A. Kuzovnikov,[1,*] Vasily S. Minkov,[2] Stella Chariton,[3] Vitali B. Prakapenka,[3] and Mikhail I. Eremets[2]

[1]*Institute of Solid State Physics RAS, 2 Academician Ossipyan Street, Chernogolovka, Moscow District 142432, Russia*

[2]*Max-Planck Institut für Chemie, Hahn-Meitner-Weg 1, 55128 Mainz, Germany*

[3]*Center for Advanced Radiation Sources, The University of Chicago, 5640 South Ellis Avenue, Chicago, Illinois 60637, USA*

(Received 5 November 2020; revised 27 November 2020; accepted 3 December 2020; published 15 December 2020)

The osmium-hydrogen system was studied at pressures up to 186 GPa by *in situ* synchrotron x-ray diffraction in a diamond anvil cell. Hydrogen solubility in the hexagonal close-packed (hcp) osmium metal at room temperature was found to be negligibly small in the studied pressure range. After laser heating of the osmium sample at the maximal H_2 pressure, it transformed to hydride with a face-centered cubic (fcc) metal lattice. The equation of state $V(P)$ for this hydride was then measured at room temperature and decreasing pressure. The hydrogen-induced volume expansion of the Os lattice proved to be weakly dependent on the pressure, and its estimated value of 1.35 $Å^3$/Os atom at 100 GPa suggested the formation of monohydride OsH with hydrogen atoms occupying all octahedral interstices in its fcc metal lattice. The OsH sample began to gradually lose hydrogen at pressures below about 55 GPa and completely decomposed to hcp-Os and molecular H_2 at about 25 GPa.

DOI: 10.1103/PhysRevB.102.214109

I. INTRODUCTION

Metal hydrides are important materials for hydrogen and energy storage applications. Superhydrides, which are a class of recently discovered hydrogen-rich compounds, are the most promising candidates for achieving room-temperature superconductivity [1–4]. The superconducting critical temperatures reach the record-high values of 146 K in hcp-ThH_9, 159–161 K in fcc-ThH_{10} [5], 203 K in bcc-H_3S [6], ∼ 220 K in bcc-YH_6 [7,8], 243 K in hcp-YH_9 [8], and 250 K in fcc-LaH_{10} [9,10].

High pressure is a very effective tool for the synthesis of new hydrogen-rich compounds, because it dramatically increases the Gibbs free energy of molecular hydrogen, stabilizing hydrides against decomposition into constituents. Some transition metals, such as group III-V elements and palladium, form hydrides already at pressures below 10^5 Pa. Chromium [11], manganese [12,13], and nickel [14] form monohydrides at pressures below 1 GPa. Most transition metals, such as Fe, Co, Mo, Tc, Rh, and Re, form monohydrides at higher hydrogen pressures of several GPa [15]. Hydrogen atoms in all monohydrides of group VI–X transition metals occupy octahedral interstitial sites in their close-packed metal lattices [15].

Recent advances in the diamond anvil cell (DAC) technique expanded the range of available hydrogen pressures to over 100 GPa in many laboratories worldwide, which led to the synthesis of a series of new compounds, such as $tI2$-CaH_4 [16,17], BaH_{12} [18], various lanthanum superhydrides [19,9], hcp-CeH_9 [20,21], hcp-PrH_9 [22] and fcc-PrH_9 [23], hcp-NdH_9 [24], hcp-EuH_9 [25], fcc-ThH_{10} [5], fcc-UH_8 [26,27], hcp-YH_9 [8], $cI16$-Zr_4H_{15} and $cI16$-Hf_4H_{15} [28], $cI16$-NbH_3 [29], $cI16$-TaH_3 [30], hcp-CrH_2 [31], hcp-MoH_{1+x} [32], hcp-WH_{1+x} [33,34], FeH_5 [35], RuH_4 [36], $sc-CoH_3$ [37], fcc-RhH_2 [38], $sc-IrH_3$ [39], Ni_2H_3 [40,41], and hcp-PtH [42]. A summary of the highest binary hydrides, which are stable at some pressure and temperature, for each element in the periodic table is given in Fig. 1.

As one can see from Fig. 1, all group IV–X transition metals except osmium have earlier been found to react with hydrogen and form hydrides at a certain pressure and temperature. Previous experimental studies revealed no reaction between Os and H_2 at pressures up to 80 GPa [43]. *Ab initio* calculations [44] predicted that OsH with a NaCl-type structure should form at hydrogen pressures above 85 GPa. Other calculations [45] predicted that the synthesis of OsH should be preceded by the formation of higher osmium hydrides in the following sequence:

$$\mathrm{Os} \overset{40\mathrm{GPa}}{\longleftrightarrow} \mathrm{OsH_6} \overset{155\mathrm{GPa}}{\longleftrightarrow} \mathrm{OsH_3} \overset{245\mathrm{GPa}}{\longleftrightarrow} \mathrm{OsH}.$$

The present paper reports on the synthesis of osmium monohydride in a DAC and the characterization of its $V(P)$ dependence and decomposition process by *in situ* x-ray powder diffraction (XRD).

II. EXPERIMENTAL

We used diamonds with a culet diameter of 40 μm, beveled at 8 ° to a diameter of about 200 μm. The gasket material was prepared from a mixture of MgO and low-viscosity epoxy resin. The gasket material was enclosed in a stainless steel holder. The thickness of the gasket was about 5 μm after indentation. The sample of a 99.95% pure osmium powder

*kuz@issp.ac.ru

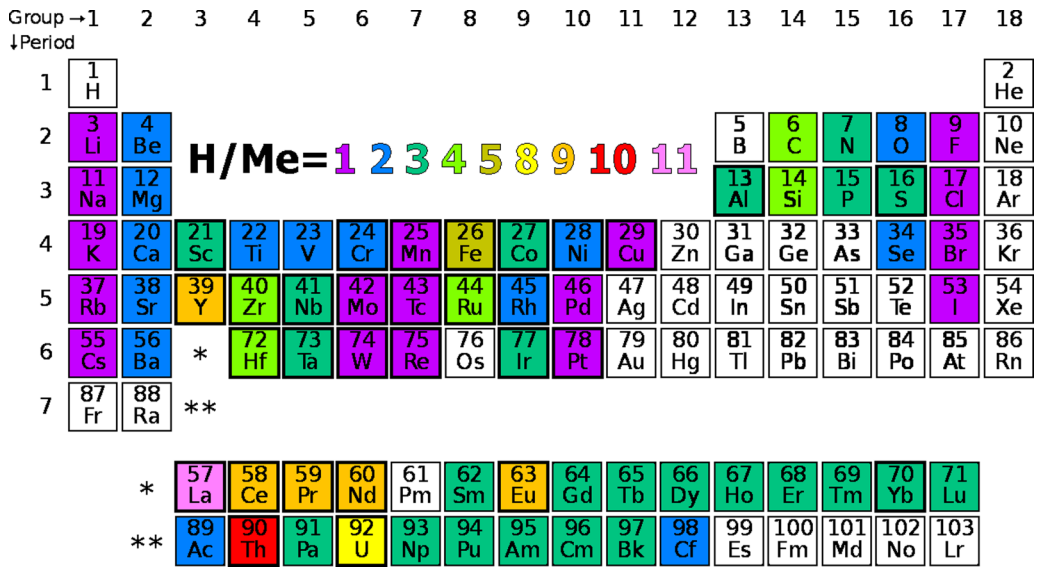

FIG. 1. Periodic table of hydrides. The cell color for each element indicates the composition of its highest hydride, which is stable at some pressure and temperature. Thick black rectangles outline elements, which highest hydride is stable at high pressure only. The compositions of nonstoichiometric hydrides are rounded off. Hydrides containing molecular H_2 units are not shown.

with a diameter of ∼15 μm was placed inside a ∼30-μm hole drilled in the gasket by a laser. The sample was handled in air.

Hydrogen was loaded into the gasket hole at room temperature and a pressure of 0.15 GPa and then served as both a reagent and a pressure-transmitting medium. Hydrogen was always in excess, and its presence in the cell throughout the experiment was monitored both visually and by Raman spectroscopy. The pressure in the cell was determined using two independent pressure scales. One scale was based on the $V(P)$ dependence for hcp-Os measured previously by XRD in quasihydrostatic medium [46], while the other was based on the well-established [47] frequency vs pressure dependence for the H_2 vibron in the Raman spectrum of molecular hydrogen surrounding the sample. Unless labeled with "$P(H_2)$", the pressures listed throughout the paper were determined with the first scale. In the studied pressure range up to 186 GPa, the difference between the two pressure scales was found to be less than 5 GPa, which is within the experimental error of Refs. [46] and [47]. This coincidence of the scales indicates the absence of a detectable hydrogen-induced volume expansion and therefore a negligibly small hydrogen solubility in hcp-Os at $P(H_2) \leqslant 186$ GPa and room temperature. In contrast, the conventional pressure scale of Akahama and Kawamura [48], based on the shift of the diamond Raman line edge, resulted in a pressure overestimation by about 25 GPa at $P(H_2) = 186$ GPa.

The XRD patterns were collected with a wavelength of 0.2952 Å and an x-ray spot size of ∼3×3 μm using a Pilatus 1M CdTe detector at the 13-IDD beamline at GSECARS, Advanced Photon Source, Argonne National Laboratory. The distance between the sample and detector, refined from the LaB_6 calibrant pattern, was about 207 mm. Primary processing and integration of the powder patterns were made using DIOPTAS v0.5.5 [49] and FIT2D v12.077 [50] software, and the POWDERCELL v2.4 [51] program was used for the Rietveld refinement.

One-sided laser heating was carried out with a pulsed YAG laser installed at the 13-IDD beamline. We performed about 20 laser heating series, gradually increasing the laser power and temperature up to 1500 K. Each series consisted of 100 000 pulses with a pulse duration of 1 μs. The temperature was determined from the thermal emission by the sample measured with a PI-MAX3 detector.

The equation of state (EoS) of the new osmium hydride and the pressure of its decomposition into hcp-Os and molecular H_2 were determined in a series of decompression steps. At each step the sample was equilibrated for about 10 min followed by its spatial XRD mapping. The mapping typically covered an 18×18 μm^2 area on the sample surface with a 7×7 set of frames, which allowed us to determine the lattice parameters of hcp-Os and fcc-OsH from the Le Bail fits of XRD profiles in the individual frames.

III. RESULTS AND DISCUSSION

After the osmium sample and H_2 gas were loaded into the DAC, the pressure was increased to $P(H_2) = 186$ GPa, as determined from the H_2 vibron position at 3943 cm^{-1}. The sample was exposed to a hydrogen atmosphere at this pressure and room temperature for about one month and then was brought to the XRD beamline. As seen from the upper red x-ray pattern in Fig. 2, the osmium sample retained its hcp crystal structure at $P(H_2) = 186$ GPa. The atomic volume of this structure is in good agreement with the extrapolation of most of the published results [46,52,53] for pure Os in inert media to this pressure. Hence osmium did not react with H_2 at room temperature.

To overcome the kinetic barrier that could prevent the absorption of hydrogen by osmium and the hydride formation, we performed a series of laser heating cycles with progressively increasing power, which raised the temperature of the sample to 1500 K and was accompanied by a drop in the

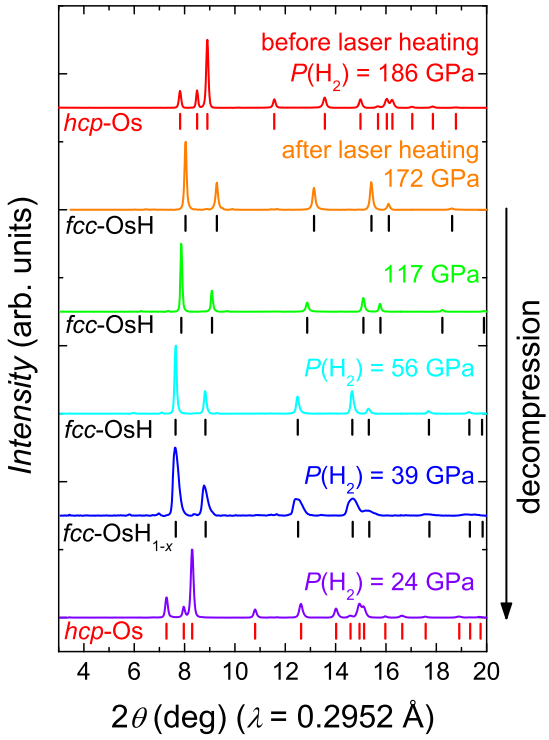

FIG. 2. XRD patterns of the Os-H_2 powder sample collected at room temperature. The upper red pattern was measured after holding the sample under the indicated H_2 pressure for one month. The orange pattern was obtained after pulsed laser heating of this sample to 1500 K. The other four patterns were collected on decompression. The pressures labeled "$P(H_2)$" were determined from the position of the hydrogen vibron, and the other pressures were determined from the $V(P)$ dependence of unreacted hcp-Os, taken from the literature [46]. The black and red ticks indicate the calculated peak positions for fcc-OsH and hcp-Os, respectively.

pressure from 186 to 172 GPa. This pressure drop could be a result of stress annealing in the gasket material and hydrogen absorption by the sample and gasket. Each heating run was followed by a spatial mapping of the sample with XRD. The final spatial mapping demonstrated that all heated parts of the sample were converted to an fcc phase with the atomic volume expanded by $\Delta V_{\rm exp}(172\ {\rm GPa}) \approx 1.2\ {\rm Å}^3/{\rm Os\ atom}$ or ≈11% compared to hcp-Os. As will be explained further in the text, the observed volume expansion suggests the formation of stoichiometric OsH.

The XRD pattern from a heated sample part obtained at 172 GPa is shown in Fig. 2 by an orange curve; results of its Rietveld refinement are presented in Fig. 3.

Le Bail refinements of the XRD patterns of osmium hydride, collected on decompression, were used to construct its $V(P)$ dependence. The obtained atomic volumes as a function of pressure are shown in Fig. 4 by open symbols. Raman spectra from the H_2 fluid were also measured after some XRD mappings and used to independently determine the pressure; the corresponding points are shown in Fig. 4 by filled symbols.

To substantiate the absence of detectable hydrogen solubility in hcp-Os and its use as a pressure marker in our experiment, we compared our x-ray results with all available $V(P)$ dependences for osmium compressed in various inert

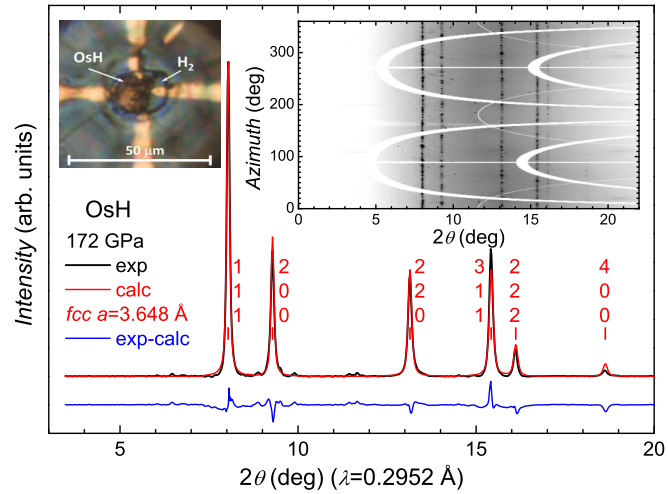

FIG. 3. Rietveld refinement of the fcc-OsH, collected after laser heating at 172 GPa. The large residual R factors, $R_p = 16.7\%$ and $R_{\rm wp} = 56\%$, are likely due to the grain effect. Left inset: sample photo after the laser heating in a combined reflection+transmission illumination. Right inset: cake representation of the detector image.

media. In Fig. 4(a), the equations of state fitted to these dependences are shown by colored curves, which are drawn solid in the experimental pressure ranges and dashed as extrapolated to higher pressures. The EoS from Ref. [54] (the red curve in Fig. 4) is likely to be the least accurate, because it considerably deviates from the other three dependences and also because the proposed pressure derivative of its bulk modulus $B_0' = 2.4$ is unrealistically low. The three experimental EoS of hcp-Os determined in Refs. [46,52,53] are close to each other

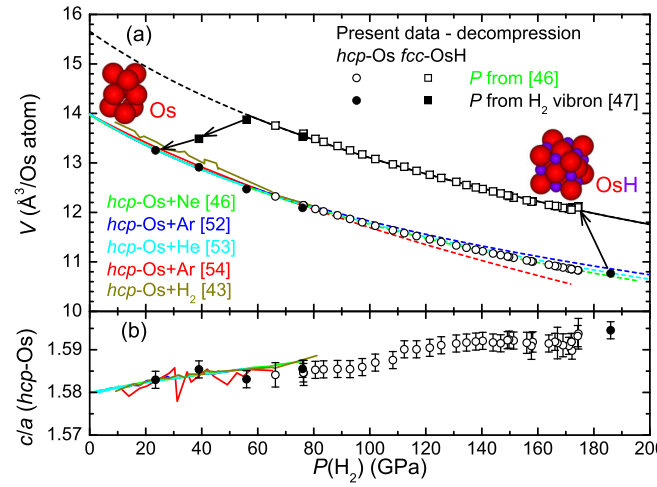

FIG. 4. Baric dependences of the atomic volume of fcc-OsH and hcp-Os (a) and the c/a ratio of hcp-Os (b). Black symbols and curves show the results of this paper; other colors are used for literature data on the compression of osmium in various inert media. The uncertainty in determining the volume is within the size of the symbols. The black curve represents the fit of the $V(P)$ data for fcc-OsH by the third-order Birch-Murnaghan equation of state with the parameters listed in Table I. The arrows indicate the formation of fcc-OsH at 172 GPa after laser heating and the gradual decomposition of this hydride on decompression from 56 to 24 GPa.

TABLE I. Fitting parameters of the Birch-Murnaghan equations of state for hcp-Os and fcc-OsH.

Substance	V_0(Å^3/M atom)	B_0(GPa)	B'_0	Source
hcp-Os	13.971(4)[a]	411(6)[a]	4.0(2)[a]	[46]
	13.989(12)	389(9)	5.0(5)	[52]
	13.988	395(15)	4.5(5)	[53]
	13.978	462(12)	2.4(0.5)	[54]
fcc-OsH	15.66(12)	393(13)	4 (fixed)	Present

[a]These parameters for hcp-Os are used presently for pressure determination.

and seem to be similar in accuracy. The EoS from Ref. [46] (the green curve in Fig. 4) was measured over a wider pressure range, and we have chosen it as the standard for determining the pressure.

As seen from Fig. 4(a), there is a good agreement between the $V(P)$ values for hcp-Os shown by the filled and open circles and obtained using, respectively, two different pressure scales, one of which was based on the position of the H_2 vibron [47], while the other one used the $V(P)$ dependence for hydrogen-free hcp osmium metal [46]. This suggests very low hydrogen solubility in hcp-Os at $P(H_2) \leqslant 186$ GPa.

Should the equilibrium hydrogen solubility in the hcp phase be considerable at this pressure, such a solution should necessarily form before the fcc hydride in areas affected by laser heating. However, the spatial mappings of the sample after the laser heating did not reveal any significant variation of the lattice parameters of the hcp phase throughout the sample, even in the two-phase hcp+fcc regions. Thus, vanishingly small hydrogen solubility in the hcp phase could not be simply attributed to a kinetic barrier for solid solution formation, and, instead, it must be an equilibrium thermodynamical effect.

In contrast, one experimental work [43] reported on a considerable hydrogen solubility in hcp-Os in the pressure range 10–50 GPa, as the authors could judge by the observed volume expansion of the order of 0.25 Å^3/Os atom [dark yellow curve in Fig. 4(a)]. However, as one can see, the volume effect and, consequently, the hydrogen solubility disappeared at $P > 50$ GPa. The decrease in the hydrogen solubility in hcp-Os with increasing pressure is a clear violation of the Le Chatelier principle, because this would increase the volume of the Os-H system. Thus the volume expansion of hcp-Os reported in Ref. [43] should be regarded as a technical artifact caused by the large uncertainty in the determination of $V(P)$ and the data scatter.

Along with the absence of the hydrogen-induced volume expansion, we also observed no difference in the c/a ratio of hcp-Os compressed in H_2 [black symbols and dark yellow curve in Fig. 4(b)] and in inert media (red, green, blue, and cyan curves). Meanwhile, this ratio is known to be very sensitive to the formation of solid solutions of hydrogen in other hcp transition metals Co, Tc, and Re [15]; for example, the formation of hcp-$ReH_{0.5}$ from hcp-Re is accompanied by a decrease in the c/a ratio from 1.613 to 1.583 [55].

The lack of noticeable hydrogen solubility in hcp-Os distinguishes the Os-H system from two other systems, Co-H [56,57] and Ru-H [58], in which the formation of fcc monohydride also occurs through the hcp→fcc transformation, but the solubility of hydrogen in the initial hcp metals gradually increases with pressure and reaches a rather large H-to-metal atomic ratio of ∼0.5 before the transformation. The reason why hcp-Os does not absorb hydrogen at pressures as high as 186 GPa is unclear.

The $V(P)$ dependence of fcc-OsH shows no anomalies at decompression down to ∼55 GPa. We fitted it to the third-order Birch-Murnaghan [59] equation of state $P(V) = \frac{3B_0}{2}\left(\left(\frac{V}{V_0}\right)^{-7/3} - \left(\frac{V}{V_0}\right)^{-5/3}\right)\left(1 + \frac{3}{4}\left(B'_0 - 4\right)\left[\left(\frac{V}{V_0}\right)^{-2/3} - 1\right]\right)$ using a value $B'_0 = 4$ of the bulk modulus pressure derivative typical of many metals, including Os [46]. We assumed the pressure P to be an independent variable and numerically solved the Birch-Murnaghan equation with respect to V for all values of the fitting parameters V_0 and B_0 and experimental P values. The resulting fit and its extrapolation to lower pressures are shown, respectively, by the solid and dashed black curves in Fig. 4(a). The obtained values of the fitting parameters for fcc-OsH and hcp-Os are compared in Table I. As one can see from Table I, the bulk moduli of hcp-Os and fcc-OsH are very close to each other, which is typical of many late transition metals and their hydrides.

Regretfully, conventional direct techniques for determining the hydrogen content, such as thermal desorption and neutron diffraction, cannot currently be used in experiments with diamond anvil cells due to the small sample size. We can, however, estimate a lower limit for the H/Os atomic ratio of the synthesized osmium hydride using the measured hydrogen-induced volume expansion $\Delta V_{exp} \approx 1.2$ Å^3/Os atom accompanying the formation of osmium hydride at 172 GPa [see Fig. 4(a)] and the known volume $^1/_2 V_{H2}(172\ \text{GPa}) \approx 1.8$ Å^3/H atom of the H_2 fluid at this pressure [60]. Since the equilibrium volume of the Os-H system (the sample plus the surrounding H_2 fluid) should always decrease with increasing pressure at constant temperature (which follows, in particular, from the Le Chatelier principle), we can write $H/Os > 2\Delta V_{exp}/V_{H2} \approx 0.67$.

As seen from Fig. 4(a), the $V(P)$ dependence for the fcc osmium hydride at $P > 56$ GPa is well approximated by the Birch-Murnaghan equation of state with constant values of V_0 and B_0. This is characteristic of hydrides with an invariable, stoichiometric H content. *Ab initio* calculations [44,45] predicted that osmium hydride with the fcc metal lattice, thermodynamically stable at high hydrogen pressures, should have a stoichiometric composition OsH and a crystal structure of the NaCl type, with H atoms at the centers of octahedral interstices of the fcc osmium lattice. Most likely, the hydride synthesized in our experiment was the predicted OsH hydride.

Figure 5 presents a comparison of the dependence $\Delta V_{exp}(P) = V_{OsH} - V_{Os}$ obtained in our work with the most reliable literature data for $\Delta V^{octa}(P)$ for monohydrides of other d metals with close-packed metal lattices, in which H atoms occupy octahedral interstices. To avoid additional uncertainty due to extrapolation of the experimental dependence $\Delta V_{exp}(P)$ for fcc-OsH to low pressures, different dependences can be compared, for example, at a hydrogen pressure of 100 GPa. As seen from Fig. 5, the point $\Delta V_{exp}(100\ \text{GPa}) = 1.35$ Å^3/Os atom for fcc-OsH (open black square) lies below the lowest point $\Delta V^{octa}(100\ \text{GPa}) \approx 1.45$ Å^3/M atom for all

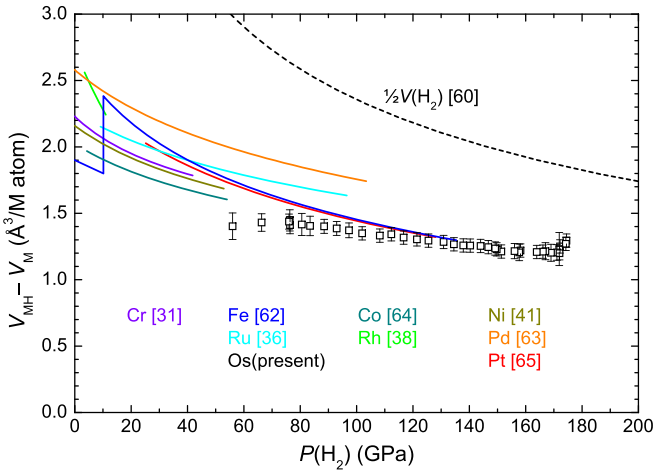

FIG. 5. Volume expansion $\Delta V^{\text{octa}}(P) = V_{\text{MH}}$–$V_{\text{M}}$ accompanying the formation of *d*-metal monohydrides MH, in which H atoms occupy octahedral interstices of the close-packed metal lattice (solid curves, literature data [31,36,38,41,62–65]); $\Delta V_{\text{exp}}(P) = V_{\text{OsH}}$–$V_{\text{Os}}$ for fcc-OsH (open black squares, results of this paper), and the equation of state of molecular hydrogen [60]. The discontinuity in the $\Delta V^{\text{octa}}(P)$ dependence for *double* hcp-FeH at $P \sim 10$ GPa is due to the bcc → hcp transformation in pure Fe.

previously studied monohydrides of *d* metals with H atoms in octahedral interstices. The occupation of tetrahedral interstices by H atoms in osmium hydride is excluded because the volume expansion in this case is expected to be approximately 1.5 times more than that for octahedral interstices [61].

The $V(P)$ dependence of fcc osmium hydride shows behavior typical of a stoichiometric compound at pressures down to approximately 56 GPa. After the measuring cell was decompressed to a lower pressure of 39 GPa, the volume of this phase continuously decreased instead of increasing [see Fig. 4(a)], and the diffraction peaks in its XRD pattern considerably broadened (see the blue curve in Fig. 2). This indicates the formation of nonstoichiometric continuous solid solutions OsH_{1-x} with the hydrogen content gradually decreasing from $H/Os \approx 1$ at $P = 56$ GPa to a lower value at $P \sim 40$ GPa. Further decrease in pressure to ~25 GPa led to the complete transformation of the fcc hydride to hcp-Os (see the violet curve in Fig. 2).

Strong dependences of the hydrogen content on pressure are characteristic of near-critical and supercritical regions of isomorphic fcc↔fcc phase transformations, which often occur between hydrogen-poor and hydrogen-rich phases in the fcc solid solutions of hydrogen in *d* metals [15,61]. In particular, a strong supercritical anomaly was observed in metastable fcc Co-H solid solutions at $P \sim 5$ GPa and $T = 325$ °C inside the $T-P$ region of thermodynamic stability of hcp Co-H solutions [56]. However, under the equilibrium conditions, the fcc cobalt hydride is formed from hcp-$CoH_{\sim 0.5}$ at a considerably higher pressure of 7.2 GPa, when its composition is already approaching CoH. Another analog of fcc osmium hydride, fcc hydride of ruthenium, also has a stoichiometric composition RuH when it is formed from hcp-$RuH_{\sim 0.5}$ at a pressure of ~14 GPa and room temperature [58]. In contrast to the Co-H and Ru-H systems, the supercritical region of the fcc↔fcc phase transformation in the Os-H system is located at higher pressures than the fcc→hcp transition.

The problem of determining the equilibrium pressure for hydride formation is essential for an accurate analysis of the thermodynamic properties of hydrides and comparing these properties with theoretical predictions. This problem is often exacerbated by the presence of large baric hysteresis between the formation and decomposition pressures of the high-pressure phases. It is generally accepted that the hysteresis is highly asymmetric in most M-H systems, with the equilibrium pressure being much closer to the decomposition pressure of the hydride with higher hydrogen content than to the midpoint between its formation and decomposition pressures (see Ref. [66] for discussion and explanation). There are several key factors accounting for the asymmetry of the hysteresis between the formation and decomposition conditions. First, the metal surface could be covered with a thin passivation oxide layer, which formed if the initial material was handled in air, as in our case. Second, the hydrogen molecules should dissociate at the metal surface before hydrogen atoms can enter the metal lattice. Third, the diffusion process of hydrogen atoms in the metal lattice could be too slow at room temperature. Moreover, the metal lattice should undergo rearrangement and expansion, which is associated with the generation of a stress comparable to yield strength. The laser heating helps to overcome the kinetic barriers associated with these factors and in our case was essential for the hydride formation. In the present experiment we did not apply laser heating at pressures below 172 GPa because of the risk of premature diamond failure, but, presumably, osmium hydride could be synthesized at much lower pressures.

Assuming that the equilibrium pressure of the reaction hcp-Os$+{}^1/_2H_2 \leftrightarrow$ fcc-OsH is $P_{eq}^{\text{H}} = 40(15)$ GPa, the standard Gibbs free energy for this reaction at $P_0 = 10^5$ Pa and $T = 298$ K can be estimated as follows:

$$\Delta G_{\text{H}}^0 = \int_{P_{eq}^{\text{H}}}^{P_0} \Delta V\, dP = \int_{P_{eq}^{\text{H}}}^{P_0} \left(V_{\text{OsH}} - V_{\text{Os}} - \tfrac{1}{2} V_{\text{H}_2}\right) dP$$
$$\approx +94(20)\ \text{kJ/mol},$$

where the $V_{\text{OsH}}(P)$ and $V_{\text{Os}}(P)$ dependences were calculated using the EoS parameters from Table I, and the $V_{\text{H}_2}(P)$ dependence was taken from Ref. [67]. Note that the standard Gibbs free energy of formation of OsH obtained in this way is much higher than $\Delta G_{\text{H}}^0(\text{RuH}) = +37(5)$ kJ/mol [58].

Due to the high Gibbs free energy of formation, it is unlikely that fcc-OsH can be recovered to ambient pressure in a metastable state, even if it is decompressed at low temperature. Nevertheless, studying the process of decomposition of fcc-Os at low temperatures would still be interesting, particularly because of the possibility to produce bulk samples of metastable fcc modification of osmium without hydrogen, which was previously observed only in nanoparticles [68].

IV. CONCLUSIONS

Using high hydrogen pressures up to 186 GPa in a DAC combined with laser heating, we synthesized hydride of osmium, which was the last group VI-X transition metal that could not be hydrogenated until now. This hydride has an fcc

metal lattice and, judging by the hydrogen-induced volume expansion, its hydrogen content approaches H/Os = 1 at pressures above ~56 GPa. Hydrogen atoms occupy octahedral interstices in the metal lattice and form a NaCl-type structure, in agreement with the prediction of *ab initio* calculations in Ref. [44]. The crystal structure of osmium hydride, its equation of state, and the process of decomposition at decreasing pressure were studied by *in situ* x-ray diffraction. The bulk modulus of fcc-OsH was close to that of hcp-Os.

The hydrogenation and dehydrogenation processes in the Os-H system were noticeably different from those in the analog systems Co-H and Ru-H studied previously. First, the solubility of hydrogen in the hcp-Os metal was negligibly small over the entire studied pressure range, while the hydrogen content of the hcp-CoH_x [56,57] and hcp-RuH_x [58] solid solutions gradually increased to $x \sim 0.5$ before the formation of fcc monohydride. Second, the fcc-OsH hydride began to gradually lose hydrogen and formed nonstoichiometric solid solutions fcc-OsH_x with $x < 1$ before decomposition into hcp-Os under decreasing pressure, while fcc-CoH and fcc-RuH remained stoichiometric phases until an abrupt transition back to the hydrogen-poor hcp phase. Third, in contrast to cobalt [37] and ruthenium [36], osmium did not form any polyhydrides with $x > 1$. Note in this connection that higher hydrides OsH_6 and OsH_3 should have been formed prior to the formation of fcc-OsH according to *ab initio* calculations in Ref. [45]. At the same time, our results are in a reasonable agreement with earlier *ab initio* predictions in Ref. [44], which gives us hope that other predicted hydrides, such as AgH [44], could be synthesized in the near future.

ACKNOWLEDGMENTS

This work was supported by RFBR Grant No. 20-02-00638 and the Max-Planck Institute for Chemistry. The synchrotron x-ray diffraction data were collected at GeoSoilEnviro CARS (The University of Chicago, Sector 13), Advanced Photon Source (APS) at Argonne National Laboratory (USA). GeoSoilEnviro CARS is supported by the National Science Foundation-Earth Sciences (EAR-1634415) and Department of Energy-GeoSciences (DE-FG02-94ER14466). This research used resources of the Advanced Photon Source, a U.S. Department of Energy (DOE) Office of Science User Facility operated for the DOE Office of Science by Argonne National Laboratory under Contract No. DE-AC02-06CH11357.

[1] H. Wang, J. S. Tse, K. Tanaka, T. Iitaka, and Y. Ma, Proc. Natl. Acad. Sci. USA **109**, 6463 (2012).
[2] Y. Li, J. Hao, H. Liu, J. S. Tse, Y. Wang, and Y. Ma, Sci. Rep. **5**, 09948 (2015).
[3] H. Liu, I. I. Naumov, R. Hoffmann, N. W. Ashcroft, and R. J. Hemley, Proc. Natl. Acad. Sci. USA **114**, 6990 (2017).
[4] F. Peng, Y. Sun, C. J. Pickard, R. J. Needs, Q. Wu, and Y. Ma, Phys. Rev. Lett. **119**, 107001 (2017).
[5] D. V. Semenok, A. G. Kvashnin, A. G. Ivanova, V. Svitlyk, V. Yu. Fominski, A. V. Sadakov, O. A. Sobolevskiy, V. M. Pudalov, I. A. Troyan, and A. R. Oganov, Mater. Today **33**, 36 (2020).
[6] A. P. Drozdov, M. I. Eremets, I. A. Troyan, V. Ksenofontov, and S. I. Shylin, Nature (London) **525**, 73 (2015).
[7] I. A. Troyan, D. V. Semenok, A. G. Kvashnin, A. V. Sadakov, O. A. Sobolevskiy, V. M. Pudalov, A. G. Ivanova, V. B. Prakapenka, E. Greenberg, A. G. Gavriliuk, V. V. Struzhkin, A. Bergara, I. Errea, R. Bianco, M. Calandra, F. Mauri, L. Monacelli, R. Akashi, and A. R. Oganov, arXiv:1908.01534.
[8] P. P. Kong, V. S. Minkov, M. A. Kuzovnikov, S. P. Besedin, A. P. Drozdov, S. Mozaffari, L. Balicas, F. F. Balakirev, V. B. Prakapenka, E. Greenberg, D. A. Knyazev, and M. I. Eremets, arXiv:1909.10482.
[9] A. P. Drozdov, P. P. Kong, V. S. Minkov, S. P. Besedin, M. A. Kuzovnikov, S. Mozaffari, L. Balicas, F. Balakirev, D. Graf, V. B. Prakapenka, E. Greenberg, D. A. Knyazev, M. Tkacz, and M. I. Eremets, Nature (London) **569**, 528 (2019).
[10] M. Somayazulu, M. Ahart, A. K. Mishra, Z. M. Geballe, M. Baldini, Y. Meng, V. V. Struzhkin, and R. J. Hemley, Phys. Rev. Lett. **122**, 027001 (2019).
[11] B. Baranowski and K. Bojarski, Ann. Soc. Chim. Polonorum **46**, 525 (1972).
[12] M. Krukowski and B. Baranowski, Ann. Soc. Chim. Polonorum **49**, 1183 (1975).
[13] E. G. Ponyatovskii and I. T. Belash, Dokl. Akad. Nauk SSSR **224**, 607 (1975) (in Russian).
[14] B. Baranowski and R. Wisniewski, Bull. Acad. Polon. Sci., Ser. Chim. **14**, 273 (1966).
[15] V. E. Antonov, J. Alloys Compd. **330-332**, 110 (2002).
[16] A. K. Mishra, T. Muramatsu, H. Liu, Z. M. Geballe, M. Somayazulu, M. Ahart, M. Baldini, Y. Meng, E. Zurek, and R. J. Hemley, J. Phys. Chem. C **122**, 19370 (2018).
[17] G. Wu, X. Huang, H. Xie, X. Li, M. Liu, Y. Liang, Y. Huang, D. Duan, F. Li, B. Liu, and T. Cui, J. Chem. Phys. **150**, 044507 (2019).
[18] W. Chen, D. V. Semenok, A. G. Kvashnin, I. A. Kruglov, M. Galasso, H. Song, X. Huang, D. Duan, A. F. Goncharov, V. B. Prakapenka, A. R. Oganov, and T. Cui, arXiv:2004.12294.
[19] Z. M. Geballe, H. Liu, A. K. Mishra, M. Ahart, M. Somayazulu, Y. Meng, M. Baldini, and R. J. Hemley, Angew. Chem. Int. Ed. **57**, 688 (2018).
[20] X. Li, X. Huang, D. Duan, C. J. Pickard, D. Zhou, H. Xie, Q. Zhuang, Y. Huang, Q. Zhou, B. Liu *et al.*, Nat. Commun. **10**, 3461 (2019).
[21] N. P. Salke, M. M. D. Esfahani, Y. Zhang, I. A. Kruglov, J. Zhou, Y. Wang, E. Greenberg, V. B. Prakapenka, J. Liu, A. R. Oganov, and J.-F. Lin, Nat. Commun. **10**, 4453 (2019).
[22] M. Peña-Alvarez, J. Binns, A. Hermann, L. C. Kelsall, P. Dalladay-Simpson, E. Gregoryanz, and R. T. Howie, Phys. Rev. B **100**, 184109 (2019).
[23] D. Zhou, D. V. Semenok, D. Duan, H. Xie, W. Chen, X. Huang, X. Li, B. Liu, A. R. Oganov, and T. Cui, Sci. Adv. **6**, eaax6849 (2020).
[24] D. Zhou, D. V. Semenok, H. Xie, X. Huang, D. Duan, A. Aperis, P. M. Oppeneer, M. Galasso, A. I. Kartsev, A. G. Kvashnin, A. R. Oganov, and T. Cui, J. Am. Chem. Soc. **142**, 2803 (2020).
[25] L. Ma, G. Liu, Y. Wang, M. Zhou, H. Liu, F. Peng, H. Wang, and Y. Ma, arXiv:2002.09900.

[26] I. A. Kruglov, A. G. Kvashnin, A. F. Goncharov, A. R. Oganov, S. S. Lobanov, N. Holtgrewe, S. Jiang, V. B. Prakapenka, E. Greenberg, and A. V. Yanilkin, Sci. Adv. **4**, eaat9776 (2018).
[27] B. Guigue, A. Marizy, and P. Loubeyre, Phys. Rev. B **102**, 014107 (2020).
[28] M. A. Kuzovnikov and M. Tkacz, J. Phys. Chem. C **123**, 30059 (2019).
[29] G. Liu, S. Besedin, A. Irodova, H. Liu, G. Gao, M. Eremets, X. Wang, and Y. Ma, Phys. Rev. B **95**, 104110 (2017).
[30] J. Ying, X. Li, E. Greenberg, V. B. Prakapenka, H. Liu, and V. V. Struzhkin, Phys. Rev. B. **99**, 224504 (2019).
[31] A. Marizy, G. Geneste, P. Loubeyre, B. Guigue, and G. Garbarino, Phys. Rev. B **97**, 184103 (2018).
[32] M. A. Kuzovnikov, H. Meng, and M. Tkacz, J. Alloys Compd. **694**, 51 (2017).
[33] H. Kawamura, T. Moriwaki, Y. Akahama, and K. Takemura, in *Proceedings of Joint 20th AIRAPT - 43rd EHPRG International Conference on High Pressure Science and Technology, Karlsruhe, 2005*, edited by E. Dinjus (Karlsruhe Institute of Technology, Karlsruhe, Germany, 2005), p. 277.
[34] T. Scheler, F. Peng, C. L. Guillaume, R. T. Howie, Y. Ma, and E. Gregoryanz. Phys. Rev. B **87**, 184117 (2013).
[35] C. M. Pépin, G. Geneste, A. Dewaele, M. Mezouar, and P. Loubeyre, Science **357**, 382 (2017).
[36] J. Binns, Y. He, M.-E. Donnelly, M. Peña-Alvarez, M. Wang, D. Y. Kim, E. Gregoryanz, P. Dalladay-Simpson, and R. T. Howie, J. Phys. Chem. Lett. **11**, 3390 (2020).
[37] M. Peña-Alvarez, B. Li, L. C. Kelsall, J. Binns, P. Dalladay-Simpson, A. Hermann, R. T. Howie, and E. Gregoryanz, J. Phys. Chem. Lett. **11**, 6420 (2020).
[38] B. Li, Y. Ding, D. Y. Kim, R. Ahuja, G. Zou, and H.-K. Mao, Proc. Natl. Acad. Sci. USA **108**, 18618 (2011).
[39] T. Scheler, M. Marqués, Z. Konôpková, C. L. Guillaume, R. T. Howie, and E. Gregoryanz, Phys. Rev. Lett. **111**, 215503 (2013).
[40] J. Ying, H. Liu, E. Greenberg, V. B. Prakapenka, and V. V. Struzhkin, Phys. Rev. Mater. **2**, 085409 (2018).
[41] J. Binns, M.-E. Donnelly, M. Wang, A. Hermann, E. Gregoryanz, P. Dalladay-Simpson, and R. T. Howie, Phys. Rev. B **98**, 140101(R) (2018).
[42] T. Scheler, O. Degtyareva, M. Marques, C. L. Guillaume, J. E. Proctor, S. Evans, and E. Gregoryanz, Phys. Rev. B **83**, 214106 (2011).
[43] T. Scheler, Ph.D. thesis, University of Edinburgh (2013).
[44] G. Gao, H. Wang, L. Zhu, and Y. Ma, J. Phys. Chem. C **116**, 1995 (2012).
[45] Y. Liu, D. Duan, X. Huang, F. Tian, D. Li, X. Sha, C. Wang, H. Zhang, T. Yang, B. Liu, and T. Cui, J. Phys. Chem. C **119**, 15905 (2015).
[46] F. Occelli, D. L. Farber, J. Badro, C. M. Aracne, D. M. Teter, M. Hanfland, B. Canny, and B. Couzinet, Phys. Rev. Lett **93**, 095502 (2004).
[47] M. I. Eremets and I. A. Troyan, Nat. Mater. **10**, 927 (2011).
[48] Y. Akahama and H. Kawamura, J. Appl. Phys. **100**, 043516 (2006).
[49] C. Prescher and V. B. Prakapenka, High Press. Res. **35**, 223 (2015).
[50] A. P. Hammersley, ESRF Internal Report ESRF97HA02T, FIT2D: An Introduction and Overview, ESRF, Grenoble, France, 1997.
[51] W. Kraus and G. Nolze, J. Appl. Cryst. **29**, 301 (1996).
[52] B. K. Godwal, J. Yan, S. M. Clark, and R. Jeanloz, J. Appl. Phys. **111**, 112608 (2012).
[53] T. Kenichi, Phys. Rev. B **70**, 012101 (2004).
[54] H. Cynn, J. E. Klepeis, C.-S. Yoo, and D. A. Young, Phys. Rev. Lett. **88**, 135701 (2002).
[55] T. Atou and J. V. Badding, J. Solid State Chem. **118**, 299 (1995).
[56] V. E. Antonov, T. E. Antonova, M. Baier, G. Grosse, and F. E. Wagner, J. Alloys Compd. **239**, 198 (1996).
[57] M. A. Kuzovnikov and M. Tkacz, J. Alloys Compd. **650**, 884 (2015).
[58] M. A. Kuzovnikov and M. Tkacz, Phys. Rev. B **93**, 064103 (2016).
[59] F. Birch, Phys. Rev. **71**, 809 (1947).
[60] P. Loubeyre, R. LeToullec, D. Hausermann, M. Hanfland, R. J. Hemley, H. K. Mao, and L. W. Finger, Nature (London) **383**, 702 (1996).
[61] Y. Fukai, *The Metal-Hydrogen System*, 2nd ed. (Springer-Verlag, Berlin, 2005).
[62] C. M. Pépin, A. Dewaele, G. Geneste, P. Loubeyre, and M. Mezouar, Phys. Rev. Lett. **113**, 265504 (2014).
[63] B. Guigue, G. Geneste, B. Leridon, and P. Loubeyre, J. Appl. Phys. **127**, 075901 (2020).
[64] M. Wang, J. Binns, M.-E. Donnelly, M. Peña-Alvarez, P. Dalladay-Simpson, and R. T. Howie, J. Chem. Phys. **148**, 144310 (2018).
[65] G. Liu, Z. Yu, S. Li, and H. Wang, Mater. Lett. **249**, 84 (2019).
[66] V. E. Antonov, A. I. Latynin, and M. Tkacz, J. Phys.: Condens. Matter **16**, 8387 (2004).
[67] J.-M. Joubert, Int. J. Hydrogen Energy **35**, 2104 (2010).
[68] T. Wakisaka, K. Kusada, T. Yamamoto, T. Toriyama, S. Matsumura, G. Ibrahima, O. Seo, J. Kim, S. Hiroi, O. Sakata, S. Kawaguchi, Y. Kubota, and H. Kitagawa, Chem. Commun. **56**, 372 (2020).